Multi-rogue wave solutions for a generalized integrable discrete nonlinear Schrödinger equation with higher-order excitations

Jun Yang · Yan-Li Zhang · Li-Yuan Ma

Abstract In this paper, we construct the discrete higher-order rogue wave (RW) solutions for a generalized integrable discrete nonlinear Schrödinger (NLS) equation. First, based on the modified Lax pair, the discrete version of generalized Darboux transformation is constructed. Second, the dynamical behaviors of first-, second- and third-order RW solutions are investigated in corresponding to the unique spectral parameter, higher-order term coefficient, and free constants. The differences between the RW solution of the higher-order discrete NLS equation and that of the Ablowitz–Ladik (AL) equation are illustrated in figures. Moreover, we explore the numerical experiments, which demonstrates that strong-interaction RWs are stabler than the weak-interaction RWs. Finally, the modulation instability of continuous waves is studied.

Keywords Generalized discrete Darboux transformation · Generalized discrete NLS equation · Higher-order RW

J. Yang
College of Arts and Sciences, Shanghai Polytechnic University, Shanghai 201209, People's Republic of China

Y.-L. Zhang · L.-Y. Ma (✉)
Department of Applied Mathematics, Zhejiang University of Technology, Hangzhou 310023, People's Republic of China
e-mail: mly2016@zjut.edu.cn

1 Introduction

Rogue wave was founded in many fields, such as nonlinear optics, fluid mechanics, and even finance [1–3]. A mass of nonlinear evolution equations including the NLS equation, Kundu–Eckhaus equation, Hirota equation, Sasa–Satuma equation, nonlinear wave equation and so on, can describe the RW phenomena [4–10]. As a basic model that describes optical soliton propagation in Kerr media, the NLS equation contains multi-soliton solutions, breather solutions, and RW solutions [5,11–13]. However, in the regime of ultra-short pulses, the NLS equation is inappropriate to accurately describe the phenomena, and higher-order nonlinear dispersion terms must be taken into account [6–9,14]. In discrete integrable system, the RW solutions of the AL equation, coupled discrete NLS equation and discrete Hirota equation are also discussed based on generalized Darboux transformation (DT) and Hirota bilinear method [15–18]. There are great differences on RWs between the continuous integrable system and discrete integrable system. Ohta and Yang point out that the RWs can exist in the defocusing Ablowitz–Ladik equation [17].

As we know, the higher-order NLS equation named as the Lakshmanan–Porsezian–Daniel (LPD) equation [19]

$$iq_t + q_{xx} + 2|q|^2 q$$
$$+ \gamma \left(q_{xxxx} + 8|q|^2 q_{xx} + 6q^* q_x^2 + 4q|q_x|^2 \right. \qquad (1)$$
$$\left. + 2q^2 q_{xx}^* + 6|q|^4 q \right) = 0.$$

is the third member of the NLS hierarchy. Here q is a varying wave packet envelope, q^* denotes the complex conjugate q, and γ is a real parameter and stands for the strength of higher-order linear and nonlinear effects. Equation (1) can also describe the dynamics of higher-order alpha-helical proteins with nearest and next nearest neighbour interactions [20,21]. This equation has attracted great attentions. In Refs. [19,22], Authors establish the relation between higher-order NLS equation and one-dimensional Heisenberg ferromagnetic chains when higher order spin-spin exchange interactions (biquadratic type) and the effect of discreteness are considered. The integrability of Eq. (1) including its singularity structure, construction of Lax pair and Bäcklund transformation have been discussed in detail in Ref. [22]. The one soliton solution of Eq. (1) has been constructed [20] by using Hirota method. Multisoliton solutions using DT is presented in [23]. Rogue waves for the three-coupled fourth-order NLS system is studied in [24]. Besides, Eq. (1) can be regarded as a special case for an integrable three-parameter fifth-order nonlinear Schrödinger equation [25,26]. Rational solutions, breather solutions, rogue wave and modulation instability of this integrable three-parameter fifth-order nonlinear Schrödinger equation are analytically studied based on DT and robust inverse scattering transform [27,28]. The corresponding rational solutions and breather solutions of Eq. (1) can be obtained under certain constraints.

In this article, we focus on the following spatial discretization [20] of integrable higher-order NLS equation (1)

$$iq_{n,t} + \frac{\gamma}{h^4}(1 + |q_n|^2) \left((1 + |q_{n-1}|^2)q_{n-2} \right.$$
$$+ (1 + |q_{n+1}|^2)q_{n+2} - 4q_{n-1} - 4q_{n+1}$$
$$+ q_n^*(q_{n+1}^2 + q_{n-1}^2) \qquad (2)$$
$$+ q_n(q_{n-1}^* q_{n+1} + q_{n-1}q_{n+1}^*) + 6q_n)$$
$$\left. + \frac{1}{h^2} \left((1 + |q_n|^2)(q_{n+1} + q_{n-1}) - 2q_n \right) = 0,$$

Equation (2) can govern the discrete α-helical protein chain model with several higher-order excitations and interactions. Under the transformation

$$q_n(t) = hq(nh, t) \triangleq hq(x, t), \qquad (3)$$

the higher-order integrable discrete NLS equation (2) yields the integrable fourth-order NLS equation (1). Reference [20] investigates the integrability of Eq. (2) including Hamiltonian, discrete Lax pair, discrete soliton and gauge equivalence. However, as we know, there is little work on rogue wave solutions and breather solutions of this higher-order integrable discrete NLS equation (2). This is the main motivation for us to investigate the higher-order RWs of the discrete integrable NLS equation (2) with higher-order excitations in this paper. Moreover, it is very meaningful to study other integrable properties of the higher-order integrable discrete NLS equation (2). We shall give an insight into the continuous limit theory of higher-order integrable discrete NLS equation (2) including discrete DT, discrete rational solutions, discrete breather solutions and gauge equivalence in the future. The paper is organized as follows. In Sect. 2, by using the modified discrete Lax pairs, we apply the generalized (1,N-1)-fold Darboux transformation [5,15] to construct higher-order discrete RW solutions of Eq. (2). The dynamical behaviors of these discrete RWs are discussed in Sect. 3, which exhibits interesting wave structures. Finally, in Sect. 4 the modulation instability of continuous-wave states of the higher-order discrete NLS equation (2) is investigated.

2 Lax pair and generalized discrete DT

The higher-order discrete NLS equation (2) admits the following discrete modified Lax pair

$$E\varphi_n = U_n\varphi_n,$$
$$\varphi_{n,t} = V_n\varphi_n, \qquad (4)$$

where the shift operator E is defined as $E\varphi_n = \varphi_{n+1}$, $\varphi_n = (\varphi_{n,1}, \varphi_{n,2})^T$ is the vector eigenfunction. The matrices U_n and V_n with spectral parameter λ take the forms

$$U_n = \begin{pmatrix} \lambda & q_n\lambda^{-1} \\ -q_n^*\lambda & \lambda^{-1} \end{pmatrix},$$
$$V_n = \frac{i\gamma}{h^4} \begin{pmatrix} A_n(\lambda, \lambda^{-1}, q_n) & B_n(\lambda, \lambda^{-1}, q_n) \\ B_n(\lambda^{-1}, \lambda, q_n^*) & -A_n(\lambda^{-1}, \lambda, q_n^*) \end{pmatrix} \qquad (5)$$
$$+ \frac{i}{h^2} \begin{pmatrix} C_n(\lambda, \lambda^{-1}, q_n) & D_n(\lambda, \lambda^{-1}, q_n) \\ D_n(\lambda^{-1}, \lambda, q_n^*) & -C_n(\lambda^{-1}, \lambda, q_n^*) \end{pmatrix},$$

in which

$$
\begin{aligned}
A_n(\lambda, \lambda^{-1}, q_n) &= \frac{\lambda^4 + \lambda^{-4}}{2} \\
&\quad + \lambda^2(q_n q_{n-1}^* - 2) + \lambda^{-2}(q_n^* q_{n-1} - 2) - 4q_n q_{n-1}^* \\
&\quad + q_n^2 q_{n-1}^{*2} + (1 + |q_{n-1}|^2)q_n q_{n-2}^* \\
&\quad + (1 + |q_n|^2)q_{n+1} q_{n-1}^* + 3, \\
B_n(\lambda, \lambda^{-1}, q_n) &= \lambda^2 q_n - \lambda^{-4} q_{n-1} \\
&\quad + (1 + |q_n|^2)q_{n+1} + q_n^2 q_{n-1}^* - 4q_n \\
&\quad - \lambda^{-2}\left((1 + |q_{n-1}|^2)q_{n-2} + q_n^* q_{n-1}^2 - 4q_{n-1}\right), \\
C_n(\lambda, \lambda^{-1}, q_n) &\\
&= \lambda^2 - 1 - (\lambda - \lambda^{-1}) + q_n q_{n-1}^*, \\
D_n(\lambda, \lambda^{-1}, q_n) &\\
&= q_n - q_{n-1}\lambda^{-2}.
\end{aligned}
$$

One can directly verify that the discrete zero curvature condition $U_{n,t} = (EV_n)U_n - U_n V_n$ of the linear spectral equations (4) yields the generalized integrable discrete NLS equation (2).

Following the idea in [29], the Darboux transformation of the higher-order discrete NLS equation (2) can be obtained. Under the gauge transformation

$$
\psi_n^{[1]} = T_n[N](\lambda)\psi_n, \tag{6}
$$

with

where $T_{n,1}^{(N-2k)}$ and $T_{n,2}^{(N-2k+1)}$ can be determined by

$$
\begin{aligned}
&\left(\lambda_j^N + \sum_{k=1}^N T_{n,1}^{(N-2k)}\lambda_j^{N-2k}\right)\varphi_{n,1}^{(j)} \\
&\quad + \left(\sum_{k=1}^N T_{n,2}^{(N-2k+1)}\lambda^{N-2k}\right)\varphi_{n,2}^{(j)} = 0, \\
&\left((\lambda_j^*)^{-N} + \sum_{k=1}^N T_{n,1}^{(N-2k)}(\lambda_j^*)^{-N+2k}\right)\varphi_{n,2}^{(j)*} \\
&\quad - \left(\sum_{k=1}^N T_{n,2}^{(N-2k+1)}(\lambda_j^*)^{-N+2k}\right)\varphi_{n,1}^{(j)*} = 0.
\end{aligned} \tag{7}
$$

The linear spectral problem (4) changes to new one as

$$
E\tilde{\psi}_n = \tilde{U}_n\psi_n, \quad \frac{\mathrm{d}\tilde{\psi}_n}{\mathrm{d}t} = \tilde{V}_n\psi_n, \tag{8}
$$

and the matrices $\tilde{U}_n$ and $\tilde{U}_n$ satisfy

$$
\tilde{U}_n = T_{n+1}[N]U_n(T_n[N])^{-1},
$$
$$
\tilde{U}_n = (T_{n,t}[N] + T_n[N]V_n)(T_n[N])^{-1},
$$

The relation between potential $\tilde{q}_n[N]$ and potential q_n is

$$
\tilde{q}_n[N] = -q_n T_{n+1,1}^{(-N)} - T_{n+1,2}^{(-N+1)}, \tag{9}
$$

where

$$
T_{n,1}^{(-N)} = -\frac{\Omega_1[N]}{\Omega[N]}, \quad T_{n,2}^{(-N+1)} = -\frac{\Omega_2[N]}{\Omega[N]}, \tag{10}
$$

$$
T_n[N] = \begin{pmatrix} \lambda^N + \sum\limits_{k=1}^N T_{n,1}^{(N-2k)}\lambda^{N-2k} & \sum\limits_{k=1}^N T_{n,2}^{(N-2k+1)}\lambda^{N-2k} \\ (-1)^{N+1}\sum\limits_{k=1}^N T_{n,2}^{(N-2k+1)*}\lambda^{-N+2k} & (-1)^N\left(\lambda^{-N} + \sum\limits_{k=1}^N T_{n,1}^{(N-2k)*}\lambda^{-N+2k}\right) \end{pmatrix},
$$

with

$$
\Omega[N] = \begin{vmatrix} \lambda_1^{-N}\varphi_{n,1}^{(1)} & \lambda_1^{-N}\varphi_{n,2}^{(1)} & \lambda_1^{-N+2}\varphi_{n,1}^{(1)} & \lambda_1^{-N+2}\varphi_{n,2}^{(1)} & \cdots & \lambda_1^{N-2}\varphi_{n,1}^{(1)} & \lambda_1^{N-2}\varphi_{n,2}^{(1)} \\ \lambda_2^{-N}\varphi_{n,1}^{(2)} & \lambda_2^{-N}\varphi_{n,2}^{(2)} & \lambda_2^{-N+2}\varphi_{n,1}^{(2)} & \lambda_2^{-N+2}\varphi_{n,2}^{(2)} & \cdots & \lambda_2^{N-2}\varphi_{n,1}^{(2)} & \lambda_2^{N-2}\varphi_{n,2}^{(2)} \\ \vdots & \vdots & \vdots & \vdots & \vdots & \vdots & \vdots \\ \lambda_N^{-N}\varphi_{n,1}^{(N)} & \lambda_N^{-N}\varphi_{n,2}^{(N)} & \lambda_N^{-N+2}\varphi_{n,1}^{(N)} & \lambda_N^{-N+2}\varphi_{n,2}^{(N)} & \cdots & \lambda_N^{N-2}\varphi_{n,1}^{(N)} & \lambda_N^{N-2}\varphi_{n,2}^{(N)} \\ (\lambda_1^*)^N\varphi_{n,2}^{(1)*} & -(\lambda_1^*)^N\varphi_{n,1}^{(1)*} & (\lambda_1^*)^{N-2}\varphi_{n,2}^{(1)*} & -(\lambda_1^*)^{N-2}\varphi_{n,1}^{(1)*} & \cdots & (\lambda_1^*)^{-N+2}\varphi_{n,2}^{(1)*} & -(\lambda_1^*)^{-N+2}\varphi_{n,1}^{(1)*} \\ (\lambda_2^*)^N\varphi_{n,2}^{(2)*} & -(\lambda_2^*)^N\varphi_{n,1}^{(2)*} & (\lambda_2^*)^{N-2}\varphi_{n,2}^{(2)*} & -(\lambda_2^*)^{N-2}\varphi_{n,1}^{(2)*} & \cdots & (\lambda_2^*)^{-N+2}\varphi_{n,2}^{(2)*} & -(\lambda_2^*)^{-N+2}\varphi_{n,1}^{(2)*} \\ \vdots & \vdots & \vdots & \vdots & \vdots & \vdots & \vdots \\ (\lambda_N^*)^N\varphi_{n,2}^{(N)*} & -(\lambda_N^*)^N\varphi_{n,1}^{(N)*} & (\lambda_N^*)^{N-2}\varphi_{n,2}^{(N)*} & -(\lambda_N^*)^{N-2}\varphi_{n,1}^{(N)*} & \cdots & (\lambda_N^*)^{-N+2}\varphi_{n,2}^{(N)*} & -(\lambda_N^*)^{-N+2}\varphi_{n,1}^{(N)*} \end{vmatrix}
$$

It is noted that the expression of $\Omega_1[N]$ and $\Omega_2[N]$ can be derived by substituting $(\lambda_1^N \varphi_{n,1}^{(1)}, \lambda_2^N \varphi_{n,1}^{(2)}, \cdots, \lambda_N^N \varphi_{n,1}^{(N)}, (\lambda_1^*)^{-N} \varphi_{n,2}^{(1)*}, (\lambda_2^*)^{-N} \varphi_{n,2}^{(2)*}, \cdots, (\lambda_N^*)^{-N} \varphi_{n,2}^{(N)*})^{\mathrm{T}}$ for the first and second column in $\Omega[N]$, respectively.

Next, we will construct the generalized $(1, N-1)$-fold DT for higher-order discrete NLS equation (2). The generalized $(1, N-1)$-fold DT links to single spectral parameter $\lambda = \lambda_1$ and the order N-1 of the highest-order derivatives for the eigenfunctions. Using the similar method in Ref. [5,18], we get a generalized $(1, N-1)$-fold DT for higher-order discrete NLS equation (2). Especially, we consider the following eigenfunction solution of the Lax pair (4) with seed solution $q_0(n, t) = c e^{i\phi t}$

$$\varphi(\lambda) = \begin{pmatrix} (C_1 \chi_1^- e^{n \ln \nu_1^- + \mu_1^- t} + C_2 \chi_1^+ e^{n \ln \nu_1^+ + \mu_1^+ t}) e^{i\phi t + \Phi(\epsilon^2)} \\ (C_1 e^{n \ln \nu_1^- + \mu_1^- t} + C_2 e^{n \ln \nu_1^+ + \mu_1^+ t}) e^{-i\phi t + \Phi(\epsilon^2)} \end{pmatrix}, \tag{11}$$

where

$$\phi = \frac{2c^2(3c^2\gamma + h^2)}{h^4},$$

$$\Phi(\epsilon^2) = \sqrt{(\lambda^2 - 1) - 4\lambda^2 c^2} \sum_{k=1}^{N}(d_k + i f_k)\epsilon^{2k},$$

$$\chi_1^\pm = \frac{1 - \lambda^2 \mp \sqrt{\lambda^4 - 2(1 + 2c^2)\lambda^2 + 1}}{2c\lambda^2},$$

$$\nu_1^\pm = \lambda + \frac{c}{\lambda \chi_1^\pm},$$

$$\mu_1^\pm = \frac{i(\lambda^2 - 1)\left(h^2\lambda^2(\lambda - 1)^2 \pm (\gamma\lambda^4 + (h^2 + 2(c^2 - 1)\gamma)\lambda^2 + \gamma)\sqrt{\lambda^4 - 2(2c^2 + 1)\lambda^2 + 1}\right)}{2h^4\lambda^4},$$

with C_j $(j = 1, 2)$ are arbitrary complex parameters (i.e., $C_1 = 1, C_2 = 0$), d_k, f_k are free real and ϵ is small parameter. We fix the spectral parameter $\lambda =$ $\lambda_1 + \epsilon^2$ with $\lambda_1 = \sqrt{1 + c^2} \pm c$ in Eq. (11) and expand eigenfunction $\varphi(\lambda)$ into the Taylor series at $\epsilon = 0$, then we obtain

$$(\lambda_1 + \epsilon^2)^j \phi_1(\lambda_1 + \epsilon^2) = \lambda_1^j \phi_1 + \phi_1[j, 1]\epsilon^2$$
$$+ \cdots + \phi_1[j, N]\epsilon^{2N} + \cdots,$$
$$(\lambda_1 + \epsilon^2)^j \psi_1(\lambda_1 + \epsilon^2) = \lambda_1^j \psi_1 + \psi_1[j, 1]\epsilon^2$$
$$+ \cdots + \psi_1[j, N]\epsilon^{2N} + \cdots, \tag{12}$$

where

$$\phi_1[j, l] = \frac{1}{(2l)!} \frac{\partial^{2l}}{\partial \epsilon^{2l}}[(\lambda_1 + \epsilon^2)^j \phi_1(\lambda_1 + \epsilon^2)]|_{\epsilon=0},$$

$$\psi_1[j, l] = \frac{1}{(2l)!} \frac{\partial^{2l}}{\partial \epsilon^{2l}}[(\lambda_1 + \epsilon^2)^j \psi_1(\lambda_1 + \epsilon^2)]|_{\epsilon=0},$$

$$j = -N, -N + 1, \ldots, 0, 1, \ldots, N$$
$$- 1, N; l = 1, 2, \ldots.$$

Then we obtain a generalized DT for the higher-order discrete NLS equation (2)

$$q_n[N] = -q_0 f_{n+1}^{(-N)} - g_{n+1}^{(-N+1)}, \tag{13}$$

where

$$f_n^{(-N)} = -\frac{\triangle_1^{[N]}}{\triangle^{[N]}}, \quad g_n^{(-N+1)} = -\frac{\triangle_2^{[N]}}{\triangle^{[N]}},$$

with

$$\triangle^{[N]} = \begin{vmatrix} \lambda^{-N-1}\phi_1 & \phi_1[-N-1,1] & \cdots & \phi_1[-N-1,N] & \lambda^{*N+1}\psi_1^* & \psi_1[N+1,1]^* & \cdots & \psi_1[N+1,N]^* \\ \lambda^{-N-1}\psi_1 & \psi_1[-N-1,1] & \cdots & \psi_1[-N-1,N] & -\lambda^{*N+1}\phi_1^* & -\phi_1[N+1,1]^* & \cdots & -\phi_1[N+1,N]^* \\ \lambda^{-N+1}\phi_1 & \phi_1[-N+1,1] & \cdots & \phi_1[-N+1,N] & \lambda^{*N-1}\psi_1^* & \psi_1[N-1,1]^* & \cdots & \psi_1[N-1,N]^* \\ \lambda^{-N+1}\psi_1 & \psi_1[-N+1,1] & \cdots & \psi_1[-N+1,N] & -\lambda^{*N-1}\phi_1^* & -\phi_1[N-1,1]^* & \cdots & -\phi_1[N-1,N]^* \\ \vdots & \vdots & \ddots & \vdots & \vdots & \vdots & \ddots & \vdots \\ \lambda^{N-1}\phi_1 & \phi_1[N-1,1] & \cdots & \phi_1[N-1,N] & \lambda^{*-N+1}\psi_1^* & \psi_1[-N+1,1]^* & \cdots & \psi_1[-N+1,N]^* \\ \lambda^{N-1}\psi_1 & \psi_1[N-1,1] & \cdots & \psi_1[N-1,N] & -\lambda^{*-N+1}\phi_1^* & -\phi_1[-N+1,1]^* & \cdots & -\phi_1[-N+1,N]^* \end{vmatrix}.$$

The matrix $\triangle_1^{[N]}$ and $\triangle_2^{[N]}$ are described by $\triangle^{[N]}$ respectively, but the first row and the second row in the $\triangle^{[N]}$ are changed to $(\lambda^{N+1}\phi_1, \ldots, \phi_1[N+1, N], \lambda^{*-N-1}\psi_1^*, \ldots, \psi_1[-N-1, N]^*)$, respectively.

3 RW solutions and dynamic behaviors

Case 1: one-order RW solutions

As $N = 1$, the solution (13) reduces

$$q_n[1] = -q_0 f_{n+1}^{(-1)} - g_{n+1}^{(0)}, \tag{14}$$

with

$$\Delta^{[1]} = \begin{vmatrix} \lambda^{-2}\phi_1 & \phi_1[-2, 1] & \lambda^{*2}\psi_1^* & \psi_1[2, 1]^* \\ \lambda^{-2}\psi_1 & \psi_1[-2, 1] & -\lambda^{*2}\phi_1^* & -\phi_1[2, 1]^* \\ \phi_1 & \phi_1[0, 1] & \psi_1^* & \psi_1[0, 1]^* \\ \psi_1 & \psi_1[0, 1] & -\phi_1^* & -\phi_1[0, 1]^* \end{vmatrix}.$$

For convenient, choose $h = 1$, $c = \frac{3}{4}$ corresponding to $\lambda_1 = \frac{1}{2}$ then we obtain the first-order RW solution of Eq. (2) is

$$q_n[1] = -\frac{3}{4} e^{\frac{9}{128}i(16+27\gamma)t}$$
$$\frac{12288n(3n-2) + 225t(8+27\gamma)(9t(8+27\gamma) - 128i) - 81920}{12288n(3n-2) + 5(4096 + 405t^2(8+27\gamma)^2)}. \tag{15}$$

Note that $q_{n+n_0}[1]$ is a solution with arbitrary real number shift n_0 and the translational property also satisfies the following higher-order RW solutions. Next we illustrate the property of first-order RW solution (15).

By analyzing the explicit formula of $q_{n+n_0}[1]$, we find that the parameter γ produces no effect in the amplitude of the first-order RW solution (15). The maximum amplitude of $|q_n[1]|$ is $\frac{63}{16}$ at point $(n_1, t_1) = (0, 0)$ with the shift $n_0 = \frac{1}{3}$, which is an on-site RW (see Fig. 1a). The minima amplitude attains 0 at two sites $(n_2, t_2) = (-1, 0)$, $(n_3, t_3) = (1, 0)$ with the shift $n_0 = \frac{4-\sqrt{21}}{3}$, $\frac{\sqrt{21}-2}{3}$ respectively. Moreover, we find that the lower peak amplitude of the first-order RW can reach at two adjacent lattice sites when $n_0 = \frac{5}{6}$, which

is called inter-site RW (see Fig.1b). Through detailed calculation, we find that the higher-order discrete NLS equation (2) has the identical amplitude but different center points with the same background wave plane comparing with the fundamental RW solution in the AL equation [17].

Next, we consider the effect of higher-order term γ and spectrum parameter λ on RWs. Figure 2a, b, c show that the first-order RWs become narrower with the increase of nonlinear term parameter γ but the peak does not changed. When $\gamma \to \infty$, the first-order RWs can concentrate the energy. On the conversely, when $\gamma \to 0$, Eq. (2) reduces to the AL equation, and the RWs approach the fundamental RWs of the AL equation. Altering the parameter λ, we see that the amplitudes of the fist-order RWs increase with the spectrum λ increase (see Fig. 2d, e).

The numerical simulation with random noise is an effective method to test the stability of the system [30,31]. In what follows, we study the dynamical behaviors of the first-order RW solutions by numerical simulation with the initial conditions and perturbation for Eq. (2). Figure 3a is the exact first-order RW solution (15). Figure 3b, c are the profiles of the numerical simulation, which exhibit the time evolution of the RWs with initial condition and the perturbation of the initial solution with 2% amplitude as random noise at $t \in (-1, 1)$, respectively. The corresponding results show that the numerical simulations of the first-order RW solution can well agree with the exact RW solution (15) besides a little weak oscillation near the edges with the perturbation case.
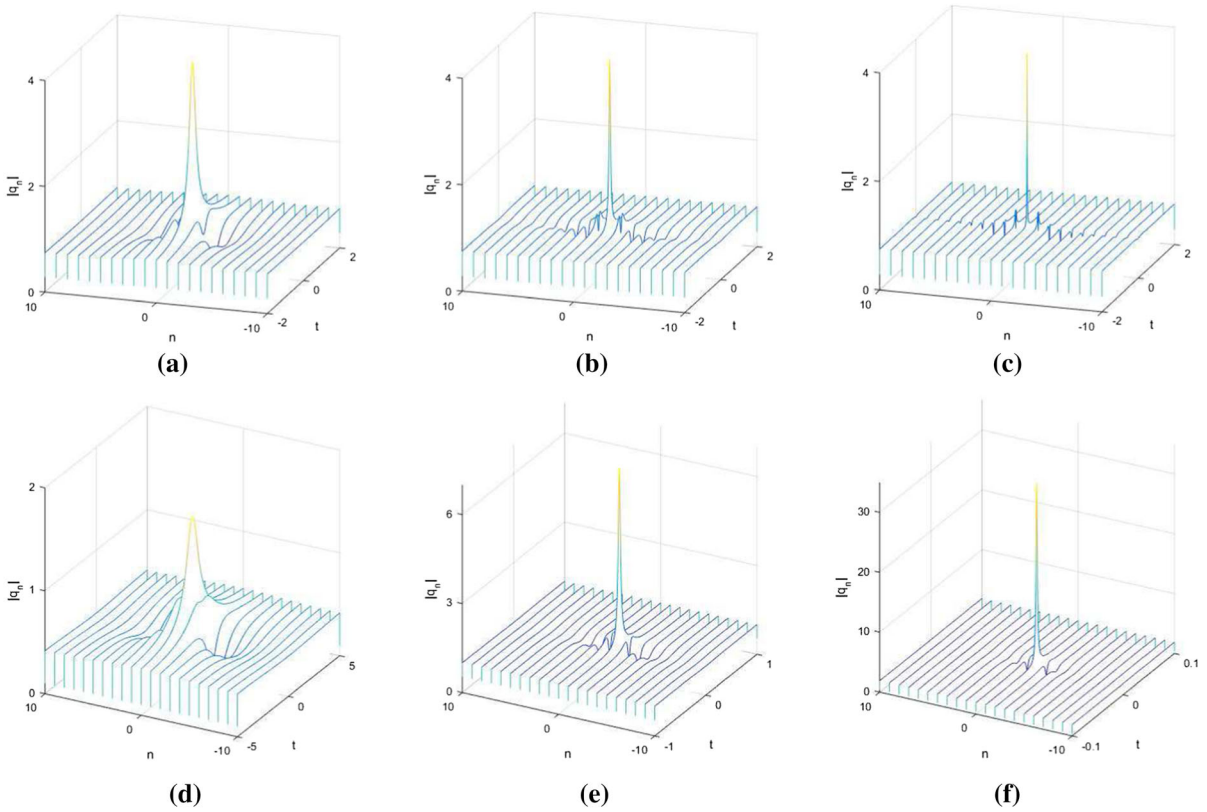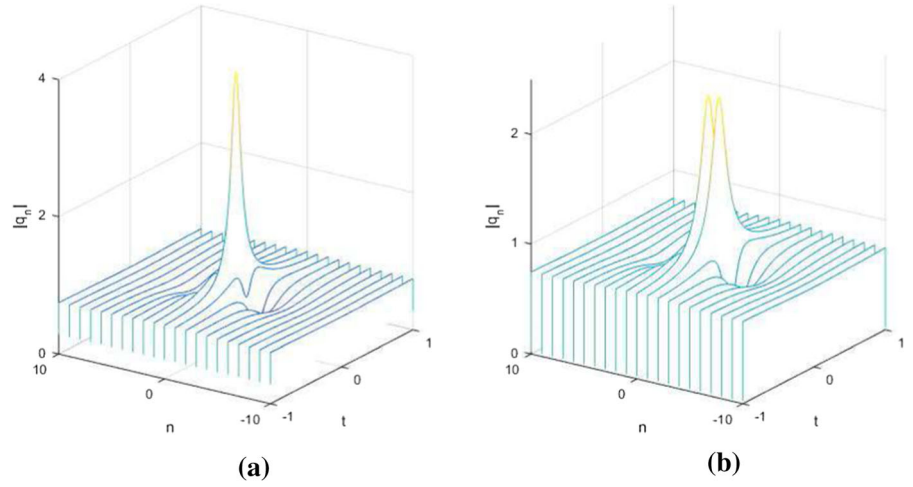
Case 2: second-order RW solutions

Formula (13) with $N = 2$ yields

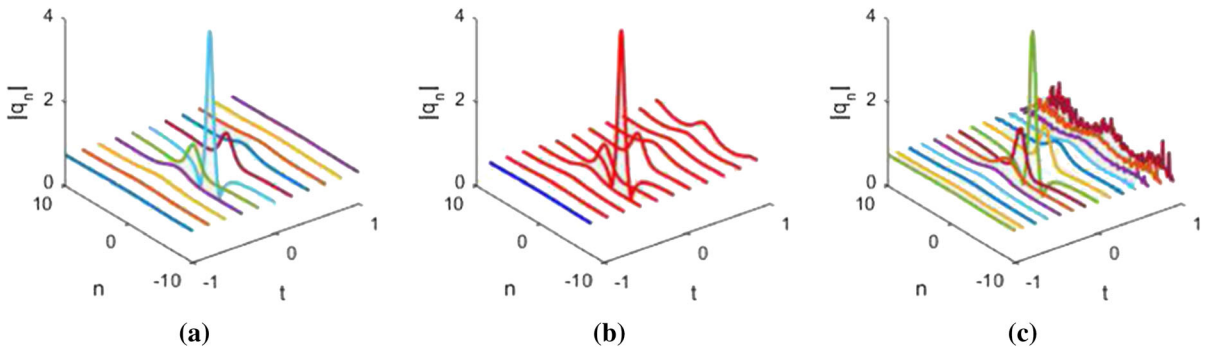$$q_n[2] = -q_0 f_{n+1}^{(-2)} - g_{n+1}^{(-1)}, \tag{16}$$

where

$$f_n^{(-2)} = -\frac{D_1^{[2]}}{D^{[2]}}, \quad g_n^{(-1)} = -\frac{D_2^{[2]}}{D^{[2]}},$$

Fig. 1 First-order RW solution (15) with $\gamma = 1$: **a** on-site RW ($n_0 = 1/3$); **b** inter-site RW ($n_0 = 5/6$)

(a)   **(b)**

(a)   **(b)**   **(c)**

(d)   **(e)**   **(f)**

Fig. 2 First-order RWs (15) with $n_0 = 1/3$ and the different parameter γ: **a** $\gamma = 1/5$; **b** $\gamma = 2$; **c** $\gamma = 10$ and plots with different parameter λ: **d** $\lambda = 2/3$, the shift $n_0 = 4/5$, **e** $\lambda = 1 + \sqrt{2}$, the shift $n_0 = (1 - \sqrt{2})/2$, **f** $\lambda = 4$, the shift $n_0 = -1/15$

Fig. 3 The first-order RW solutions (15). **a** Exact solution, **b** numerical simulations using exact solutions (15) with $t = -1$. **c** numerical simulations by adding random noise with amplitude 2% as the initial condition

with

$$\Delta^{[2]} = \begin{vmatrix} \lambda^{-3}\phi_1 & \phi_1[-3,1] & \phi_1[-3,2] & \lambda^{*3}\psi_1^* & \psi_1[3,1]^* & \psi_1[3,2]^* \\ \lambda^{-3}\psi_1 & \psi_1[-3,1] & \psi_1[-3,2] & -\lambda^{*3}\phi_1^* & -\phi_1[3,1]^* & -\phi_1[3,2]^* \\ \lambda^{-1}\phi_1 & \phi_1[-1,1] & \phi_1[-1,2] & \lambda^*\psi_1^* & \psi_1[1,1]^* & \psi_1[1,2]^* \\ \lambda^{-1}\psi_{-1} & \psi_1[-1,1] & \psi_1[-1,2] & -\lambda^*\phi_1^* & -\phi_1[1,1]^* & -\phi_1[1,2]^* \\ \lambda\phi_1 & \phi_1[1,1] & \phi_1[1,2] & \lambda^{*-1}\psi_1^* & \psi_1[-1,1]^* & \psi_1[-1,2]^* \\ \lambda\psi_1 & \psi_1[1,1] & \psi_1[1,2] & -\lambda^{*-1}\phi_1^* & -\phi_1[-1,1]^* & -\phi_1[-1,2]^* \end{vmatrix},$$

and $\Delta_1^{[2]}$ and $\Delta_2^{[2]}$ are described by $\Delta^{[2]}$, but the first row and the second row are replace by $(\lambda_1^3\phi_1, \phi_1[3,1], \phi_1[3,2], \lambda_1^{*-3}\psi_1^*, \psi_1[-3,1]^*, \psi_1[-3,2]^*)$ in the $\Delta^{[2]}$, respectively.

If we choose $c = 3/4, \lambda = 2, h = \gamma = 1$, the exact second-order RW solutions can be expressed as

$$q_n[2] = -\frac{3}{4}e^{\frac{387}{128}it}\frac{A_2(n,t)}{B_2(n,t)}\bigg|_{n\to n+n_0} \tag{17}$$

where $B_2(n,t)$, $A_2(n,t)$ are obtained through mathematica software:

$B_2(n,t) = 68719476736(1600 + 3n(1280 + 3n(497$
$\quad + 3n(136 + 3n(26 + n(8 + n)))))) + 849346560000(23465$
$\quad + 21n(-2056 + 3n(-96 + 7n(16 + 3n))))t^2$
$\quad + 1200225600000000(670 + 21n(8 + 3n))t^4$
$\quad + 1696058545166015625t^6 + 1061683200$
$(25t(4096(-125 + 21n(8 + 3n)) - 5788125t^2)d_1$
$\quad + 3276800d_1^2 + 64e_1(4096n(1 + n)(3 + n)$
$\quad - 275625(4 + 3n)t^2 + 51200e_1)),$
$A_2(n,t) = 68719476736(100 + 3n(-1520 + 3n(-428$
$\quad + n(8 + 3n(53 + 3n(8 + n))))))) - 2415919104000i(-4880$

$\quad + 3n(-1336 + 3n(-6 + 7n(16 + 3n))))t$
$\quad + 2548039680000(-29220 + 7n(-4856 + 3n(-446$
$\quad + 7n(16 + 3n))))t^2 - 975421440000000i$
$(275 + 21n(8 + 3n))t^3 + 1200225600000000(-205$
$\quad + 21n(8 + 3n))t^4 - 20675761312500000000it^5$
$\quad + 1696058545166015625t^6 + 589824000($
$\quad - 262144i(20 + 3n(8 + 3n)) + 184320(50 + 21n(8$
$\quad + 3n))t + 158760000it^2 - 260465625t^3)d_1$
$\quad + 3478923509760000d_1^2$
$\quad + 7549747200e_1(4096(100 + 3n(34 + 3n(4 + n)))$
$\quad + 1008000i(4 + 3n)t$
$\quad - 2480625(4 + 3n)t^2 + 460800e_1).$

We see that the parameters d_1 and f_1 control the strong and weak interaction of the second-order RW (17).

• For the case $d_1 = f_1 = 0$, the strong interaction happens that the RWs have four minimum points and five local maximum including a biggest peak at the center of the wave packets (see Fig. 4a).
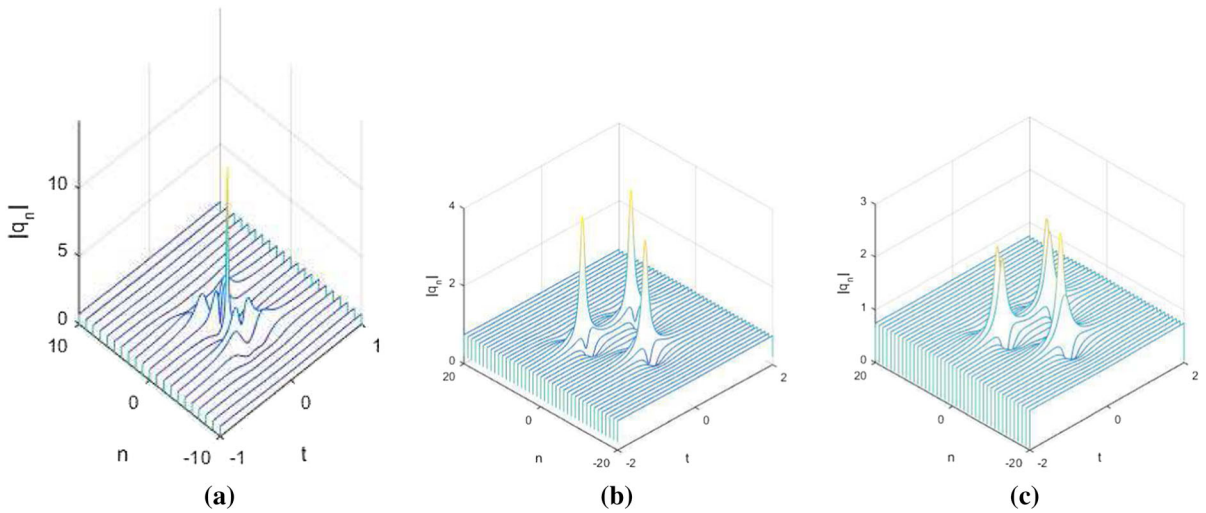
Fig. 4 The second-order discrete RW solutions (17) with $c = 3/4$, $\lambda=2$, $h = \gamma = 1$. **a** $d_1 = f_1 = 0$, $n_0 = 0$; **b** $d_1 = 10$, $f_1 = 0$, $n_0 = -5/6$; **c** $d_1 = 0$, $f_1 = 10$, $n_0 = 2/3$

• For the case $d_1 \neq 0$ or $f_1 \neq 0$, the second-order RWs split into three first-order RWs, whose centers become a rotating triangle, and the whole profiles have three local maximum and six minimum points (see Fig. 4b, c).

Moreover, adjusting the parameters freely, we find that the area of the triangle increases with the increase of the parameters $|d_1|$ or $|f_1|$ and $|f_1|$ can control the rotation of the triangle RWs.

Next, we give the dynamical property for the second-order RWs by the numerical simulation. Figure 5a, d are exact second-order RW solutions with different parameters d_1 and e_1. Figure 5b, c show that the numerical simulation of the strong interaction (i.e., $d_1 = 0$, $f_1 = 0$) can well agree with the exact solution except for weak oscillations at $t > 0.4$ (see Fig. 5c). For the weak

interaction case (i.e., $d_1 = 10$, $f_1 = 0$), we find that the wave propagation can also match the exact solution well. However, if we add the random noise (2%) to the initial solution, the weak interaction displays serious oscillations after time exceeds 0.2, which may be due to the main energy distribution [17].

Case 3: third-order RW solutions

When $N = 3$, by the formula (13) and take the special spectral parameters $\lambda = \frac{7}{4}$ with $c = \frac{33}{56}$, then the third-order discrete RW solution is obtained as

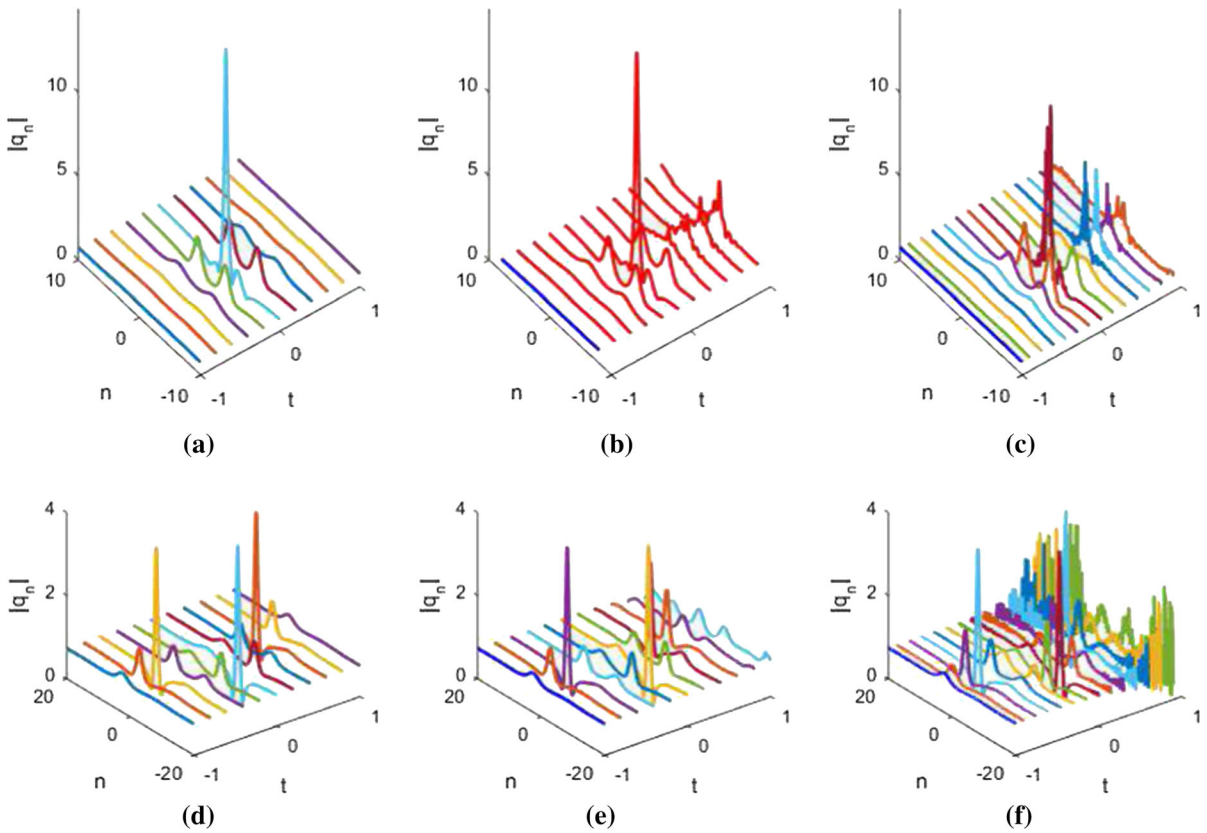$$q_n[3] = -q_0 f_{n+1}^{(-3)} - g_{n+1}^{(-2)}, \tag{18}$$

where

$$f_n^{(-3)} = -\frac{\Delta_1^{[3]}}{\Delta^{[3]}}, \quad g_n^{(-2)} = -\frac{\Delta_2^{[3]}}{\Delta^{[3]}},$$

with

$$\Delta^{[3]} = \begin{vmatrix} \phi_1[-4,0] & \phi_1[-4,1] & \phi_1[-4,2] & \phi_1[-4,3] & \psi_1[4,0]^* & \psi_1[4,1]^* & \psi_1[4,2]^* & \psi_1[4,3]^* \\ \psi_1[-4,0] & \psi_1[-4,1] & \psi_1[-4,2] & \psi_1[-4,3] & -\phi_1[4,0]^* & -\phi_1[4,1]^* & -\phi_1[4,2]^* & -\phi_1[4,3]^* \\ \phi_1[-2,0] & \phi_1[-2,1] & \phi_1[-2,2] & \phi_1[-2,3] & \psi_1[2,0]^* & \psi_1[2,1]^* & \psi_1[2,2]^* & \psi_1[2,3]^* \\ \psi_1[-2,0] & \psi_1[-2,1] & \psi_1[-2,2] & \psi_1[-2,3] & -\phi_1[2,0]^* & -\phi_1[2,1]^* & -\phi_1[2,2]^* & -\phi_1[2,3]^* \\ \phi_1[0,0] & \phi_1[0,1] & \phi_1[0,2] & \phi_1[0,3] & \psi_1[0,0]^* & \psi_1[0,1]^* & \psi_1[0,2]^* & \psi_1[0,3]^* \\ \psi_1[0,0] & \psi_1[0,1] & \psi_1[0,2] & \psi_1[0,3] & -\phi_1[0,0]^* & -\phi_1[0,1]^* & -\phi_1[0,2]^* & -\phi_1[0,3]^* \\ \phi_1[2,0] & \phi_1[2,1] & \phi_1[2,2] & \phi_1[2,3] & \psi_1[-2,0]^* & \psi_1[-2,1]^* & \psi_1[-2,2]^* & \psi_1[-2,3]^* \\ \psi_1[2,0] & \psi_1[2,1] & \psi_1[2,2] & \psi_1[2,3] & -\phi_1[-2,0]^* & -\phi_1[-2,1]^* & -\phi_1[-2,2]^* & -\phi_1[-2,3]^* \end{vmatrix},$$

Fig. 5 The second-order RW solutions (17). Exact solutions with **a** $d_1 = f_1 = 0$ and **d** $d_1 = 10, = f_1 = 0$. **b** and **e** the numerical simulation using exact solutions (17) at $t = -1$ as initial conditions. **d** and **f** numerical simulations by adding random noise with amplitude 2% to the exact solutions (17) as initial conditions

and $\Delta_1^{[3]}$ and $\Delta_2^{[3]}$ change to $\Delta^{[3]}$ but the first row and second row in the $\Delta^{[3]}$ are replaced by $(\phi_1[4, 0], \phi_1[4, 1], \phi_1[4, 2], \phi_1[4, 3], \psi_1[-4, 0]^*, \psi_1[-4, 1]^*, \psi_1[-4, 2]^*, \psi_1[-4, 3]^*)$, respectively. The exact expression of three-order RW solution is so clumsy that we omit it here.

We just give its structural analysis corresponding to the four different parameters $(d_{1,2}, f_{1,2})$.

• For the case $d_{1,2} = f_{1,2} = 0$, the strong intera——ction is displayed in Fig. 6a.

The weak interaction happens when $d_1 \neq 0$ or $d_2 \neq 0$, $f_{1,2} = 0$.

• For the case $d_1 = 10, d_2 = f_{1,2} = 0$, the third-order RWs split into six first-order RWs, which form a triangular pattern (see Fig. 6b);

• For the case $d_2 = 10, d_1 = f_{1,2} = 0$, the third-order RWs also split into six first-order RWs, which array to a rotating pentagon pattern with a first-order RWs located at the center (see Fig. 6c).

Now we study the dynamical behaviors for the third-order RWs (18) by the numerical simulation. Here, we only consider the strong-interaction case (see Fig. 6a) and weak interaction case (see Fig. 6b). Figure 7a, b show that the strong-interactions of third-order RWs almost agree with the exact solution (18). If a small noise adds to the exact solution (18) in strong-interaction case, the wave propagation behaves well except a small bulge around the edges (see Fig. 7c) but the amplitude is obviously lower than the one's of the exact solution and numerical simulation case (see Fig. 7a, b). On the other hand, no matter what we add a noise or not to the initial condition, the wave propagations of weak interaction of third-order RWs display strong oscillations (see Fig. 7d–f). We infer that the dispersed energy of the third-order RWs can more easily lead to the disorder than the strong interaction case.
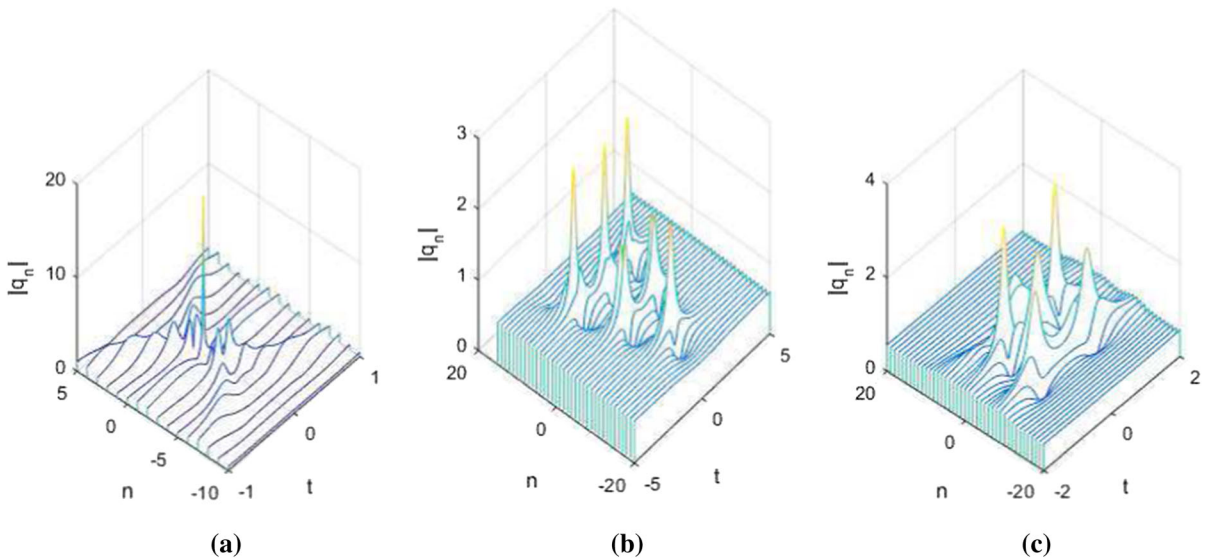
Fig. 6 Third-order discrete RW solutions with $h = \gamma = 1$ **a** strong interaction $d_{1,2} = f_{1,2} = 0$, $n_0 = 0$; **b** a triangular pattern with $d_1 = 10$, $d_2 = 0$, $f_{1,2} = 0$, $n_0 = -1/2$; **c** a pentagon pattern with $d_1 = 0$, $d_2 = 10$, $f_{1,2} = 0$, $n_0 = -1/3$

4 Modulation instability of continuous-wave states

Many studies [32–35] have shown that the modulational instability (MI) associated with the growth of perturbations on a plane wave background can result in the RWs. We consider the continuous-wave solution of Eq. (2) with $q_0(n, t) = ce^{i\phi t}$, where the real amplitude $c \neq 0$. We perturb this solution

$$q_n(t) = \left(1 + \frac{\varepsilon}{c}\hat{q}_n(t)\right) q_0(n, t), \tag{19}$$

where ε is an infinitesimal amplitude and $\hat{q}_n(t)$ is a perturbation solution. Substituting (19) into Eq. (2) yields a complex linearized equation

$$i\hat{q}_{n,t} + \gamma(1 + c^2)^2\hat{q}_{n-2} + (1 + c^2 + 4\gamma(c^2 - 1))\hat{q}_{n-1}$$
$$+ (2\gamma(c^2 + 1)(c^2 - 3) - 2)\hat{q}_n + \gamma(c^2 + 1)^2\hat{q}_{n+2}$$
$$+ (c^2 + 1)(4\gamma(c^2 - 1) + 1)\hat{q}_{n+1} + 2c^2\gamma(1 + c^2)\hat{q}_{n-1}^*$$
$$+ 2c^2(1 - 2\gamma + 4c\gamma)\hat{q}_n^* + 2c^2\gamma(1 + c^2)\hat{q}_{n+1}^* = 0. \tag{20}$$

$$\gamma(1 + c^2)^2 q_{1,n-2} + (1 + c^2)(1 - 4\gamma + 6\gamma c^2)q_{1,n-1}$$
$$+ 2(-1 + c^2 + \gamma(3 - 4c^2 + 5c^4))q_{1,n}$$
$$+ (1 + c^2)\gamma(-4 + 6c^2))q_{1,n+1}$$
$$+ (1 + c^2)^2 q_{1,n+2} - q_{2,n,t} = 0,$$
$$(1 + c^2)[\gamma(1 + c^2)q_{2,n-2} + (1 + 2\gamma(c^2 - 2))q_{2,n-1}$$
$$- 2(1 + 3\gamma(c^2 - 1))q_{2,n}$$
$$+ (1 + 2\gamma(c^2 - 2))q_{2,n+1}$$
$$+ \gamma(1 + c^2)q_{2,n+2}] + q_{1,n,t} = 0. \tag{21}$$

Assume that real equation (21) exists the following complex solution

$$(q_{1,n}(t), q_{2,n}(t)) = (q_{1,n}^{(0)}, q_{2,n}^{(0)})e^{gt+ikn}, \tag{22}$$

where g is the MI gain k is an arbitrary real wavenumber and $q_{1,n}^{(0)}$, $q_{2,n}^{(0)}$ are constant amplitudes of the perturbation eigenmode. Substituting (22) into Eq. (21) yields the MI dispersion equation in the form of the determinant

$$\begin{vmatrix} -g & 2(c^2 - 1 + (c^2+1)\cos k)(1 + 2\gamma(2c^2 - 1) + 2\gamma(c^2 + 1)\cos k) \\ -4(c^2 + 1)(1 + 2\gamma(c^2 - 1) + 2\gamma(c^2 + 1)\cos k)\sin^2\frac{k}{2} & g \end{vmatrix} = 0, \tag{23}$$

We consider the perturbation with real and imaginary parts $\hat{q}_n = q_{1,n}(t) + iq_{2,n}(t)$, which changes the complex linearized equation can change into two real equations

which gives an explicit dispersion relation

$$g^2 = 8(1 + c^2)\left(c^2 - 1 + (c^2 + 1)\cos k\right)$$
$$\left(1 + 2\gamma(2c^2 - 1) + 2\gamma(1 + c^2)\cos k\right)^2 \sin^2\frac{k}{2}. \tag{24}$$
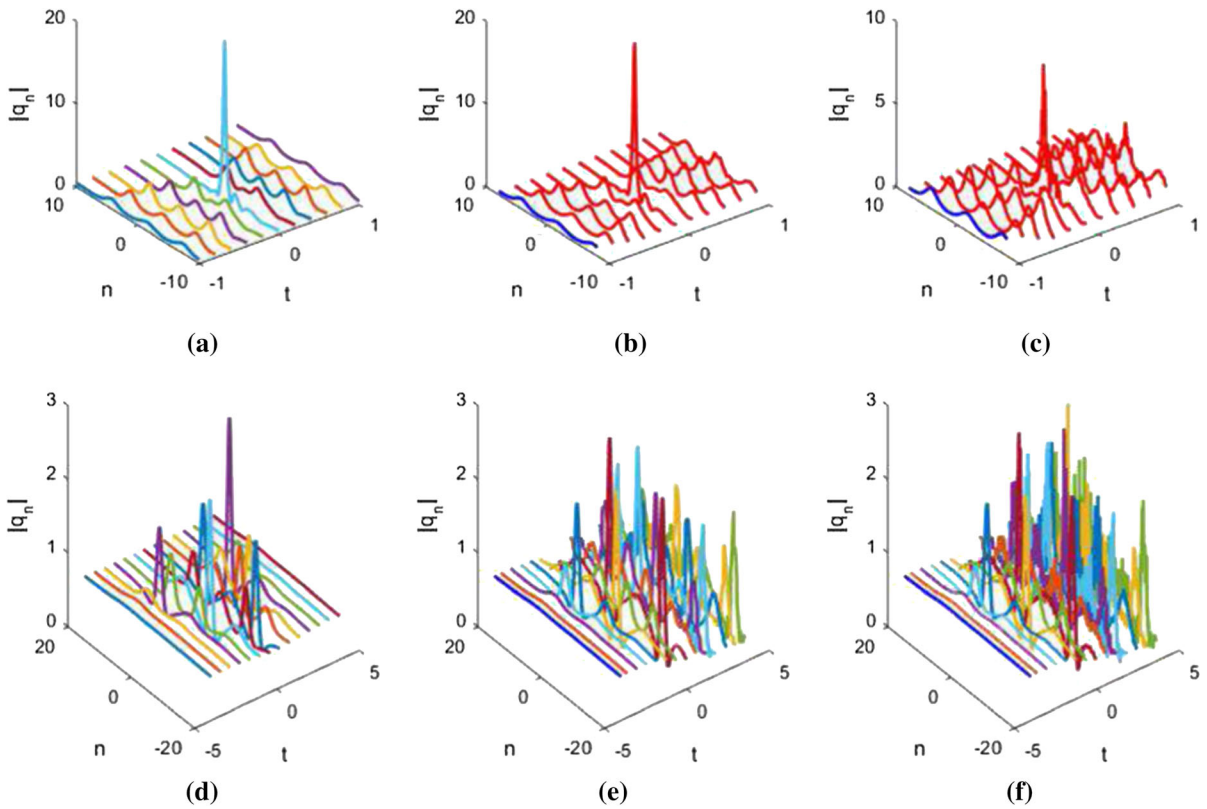
Fig. 7 The third-order RW solutions (18). The exact solution **a** $d_{1,2} = f_{1,2} = 0$ and **d** $d_1 = 10, d_2 = f_{1,2} = 0$ (left); **b** and **e** simulated simulation using exact solutions (18) as the initial conditions (middle); **c** and **f** numerical simulations by adding random noise with amplitude 2% to the exact solutions (18) as initial conditions (right)

Fig. 8 Gain spectra of the MI for different CW amplitude c and higher order parameter γ. **a** Different amplitude with $c = 2$ (blue solid), $c = 3$ (red dashed), and $c = 4$ (green dotted-dashed); **b** Different parameter with $\gamma = 1$ (blue solid), $\gamma = 2$ (red dashed), and $\gamma = 3$ (green dotted-dashed)
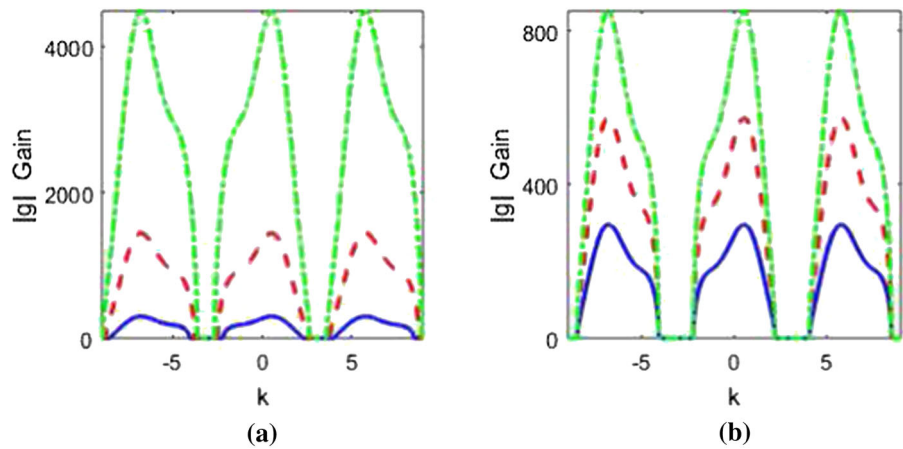
We point out here the MI takes place when expression (24) is positive. The MI condition $g^2 > 0$ holds as

$$\cos k > \frac{1 - c^2}{1 + c^2},$$
$$\cos k \neq -\frac{1 + 2\gamma(2c^2 - 1)}{2\gamma(1 + c^2)}, \text{ and}$$
$$k \neq 2m\pi, m \in Z.$$

Figure 8 shows that the growth rate $g(k)$ becomes larger and larger as the amplitude c increases, meanwhile, for the fixed amplitude $c = 2$, $g_{\max}(k)$ also gets larger with the increase of parameter γ.

5 Conclusions

In this paper, we have studied a higher-order integrable discrete NLS equation by the generalized discrete $(1, N - 1)$-fold Darboux transformation. The discrete higher-order RW solutions are given by determinants. We have analytically studied the dynamical behaviors of discrete RW solutions, which exhibits abundant patterns including on-site, inter-site, the rotating triangle and pentagon structures. Comparing with the discrete NLS equation, the first-order RWs of integrable higher-order discrete NLS equation have the identical peaks but different center points with the same plane-wave amplitude. We also find that the nonlinear term parameter γ can control energy density of the RWs. By means of numerical simulation with the time evolutions of the RW solutions, we reveal that the strong interaction RWs are more stable on the wave propagation than the weak interaction case. Finally, the modulation instability condition of the background wave solutions are given.

Data availability All data generated or analysed during this study are including in this published article.

Declarations

Conflict of interest The authors declare that they have no conflict of interest.

References

1. Solli, D.R., Ropers, C., Koonath, P., Jalali, B.: Optical rogue waves. Nature **450**, 06402 (2007)
2. Chabchoub, A., Hoffmann, N.P., Akhmediev, N.: Rogue wave observation in a water wave tank. Phys. Rev. Lett. **106**, 204502 (2011)
3. Yan, Z.Y.: Vector financial rogue waves. Phys. Lett. A **375**, 4274–4279 (2011)
4. Akhmediev, N., Ankiewicz, A., Taki, M.: Waves that appear from nowhere and disappear without a trace. Phys. Lett. A **373**, 675–678 (2009)
5. Guo, B.L., Ling, L.M., Liu, Q.P.: Nonlinear Schrödinger equation: generalized Darboux transformation and rogue wave solutions. Phys. Rev. E **85**, 026607 (2012)
6. Tao, Y.S., He, J.S.: Multisolitons, breathers, and rogue waves for the Hirota equation generated by the Darboux transformation. Phys. Rev. E **85**, 026601 (2012)
7. Qiu, D.Q., He, J.S., Zhang, Y.S., Porsezian, K.: The Darboux transformation of the Kundu–Eckhaus equation. Proc. R. Soc. A **471**, 20150236 (2015)
8. Wang, M.M., Chen, Y.: Dynamic behaviors of mixed localized solutions for the three-component coupled Fokas–Lenells system. Nonlinear Dyn. **98**, 1781–1794 (2019)
9. Soto-Crespo, J.M., Devine, N., Hoffmann, N.P., Akhmediev, N.: Rogue waves of the Sasa–Satsuma equation in a chaotic wave field. Phys. Rev. E **90**, 032902 (2014)
10. Wang, M., Tian, B., Sun, Y., Zhang, Z.: Lump, mixed lump-stripe and rogue wave-stripe solutions of a (3+1)-dimensional nonlinear wave equation for a liquid with gas bubbles. Comput. Math. Appl. **79**, 576–582 (2020)
11. Porsezian, K., Nakkeeran, K.: Optical solitons in presence of Kerr dispersion and self-frequency shift. Phys. Rev. Lett. **78**, 3227 (1997)
12. Akhmediev, N., Eleonskii, V.M., Kulagin, N.E.: Exact first-order solutions of the nonlinear Schrödinger equation. Theor. Math. Phys. **72**, 809–818 (1987)
13. Ma, Y.C.: The perturbed plane-wave solutions of the cubic Schrödinger equation. Stud. Appl. Math. **60**, 43–59 (1979)
14. Feng, B.F.: Complex short pulse and coupled complex short pulse equations. Physica D **297**, 15 (2015)
15. Wen, X.Y., Yan, Z.Y., Malomed, B.A.: Higher-order vector discrete rogue-wave states in the coupled Ablowitz–Ladik equations: exact solutions and stability. Chaos **26**, 123110 (2016)
16. Wen, X.Y., Yan, Z.Y.: Modulational instability and dynamics of multi-rogue wave solutions for the discrete Ablowitz–Ladik equation. J. Math. Phys. **59**, 073511 (2018)
17. Ohta, Y., Yang, J.K.: General rogue waves in the focusing and defocusing Ablowitz–Ladik equations. J. Phys. A: Math. Theor. **47**, 255201 (2014)
18. Yang, J., Zhu, Z.N.: Higher-order rogue wave solutions to a spatial discrete Hirota equation. Chin. Phys. Lett. **35**, 090201 (2018)
19. Lakshmanan, M., Porsezian, K., Daniel, M.: Effect of discreteness on the continuum limit of the Heisenberg spin chain. Phys. Lett. A **133**(9), 483–488 (1988)
20. Daniel, M., Latha, M.M.: Soliton in discrete and continuum alpha helical proteins with higher-order excitations. Phys. A **240**, 526–546 (1997)

21. Daniel, M., Latha, M.M.: A generalized Davydov soliton model for energy transfer in alpha helical proteins. Phys. A **298**, 351–370 (2001)

22. Porsezian, K., Daniel, M., Lakshmanan, M.: On the integrability aspects of the one dimensional classical continuum isotropic biquadratic Heisenberg spin chain. J. Math. Phys. **33**, 1807–1816 (1992)

23. Veni, S.S., Latha, M.M.: Nonlinear excitations in a disordered alpha-helical protein chain. Phys. A **407**, 76–85 (2014)

24. Du, Z., Tian, B., Chai, H.P., Zhao, X.H.: Lax pair, Darboux transformation and rogue waves for the three-coupled fourth-order nonlinear Schrödinger system in an alpha helical protein. Wave Random Complex (2019). https://doi.org/10.1080/17455030.2019.1644466

25. Kano, T.: Normal form of nonlinear Schrödinger equation. J. Phys. Soc. Jpn. **58**, 4322–4328 (1989)

26. Chowdury, A., Kedziora, D.J., Ankiewicz, A., Akhmediev, N.: Soliton solutions of an integrable nonlinear Schrödinger equation with quintic terms. Phys. Rev. E **90**, 032922 (2014)

27. Yang, Y.Q., Yan, Z.Y., Malomed, B.A.: Rogue waves, rational solitons, and modulational instability in an integrable fifth-order nonlinear Schrödinger equation. Chaos **25**, 103112 (2015)

28. Chen, S.Y., Yan, Z.Y.: The higher-order nonlinear Schrödinger equation with non-zero boundary conditions: robust inverse scattering transform, breathers, and rogons. Phys. Lett. A **383**, 125906 (2019)

29. Pickering, A., Zhao, H.Q., Zhu, Z.N.: On the continuum limit for a semidiscrete Hirota equation. Proc. Roy. Soc. A: Math., Phys. Eng. Sci. **472**, 20160628 (2016)

30. Saravanakumar, T., Marshal Anthoni, S., Zhu, Q.X.: Resilient extended dissipative control for Markovian jump systems with partially known transition probabilities under actuator saturation. J. Frankl. **I**(357), 6197–6227 (2020)

31. Saravanakumar, T., Muoi, N.H., Zhu, Q.X.: Finite-time sampled-data control of switched stochastic model with non-deterministic actustor faults and saturation nonlinearity. J. Frankl. **I**(357), 13637–13665 (2020)

32. Dudley, J.M., Genty, G., Dias, F., Kibler, B., Akhmediev, N.: Modulation instability, Akhmediev breathers and continuous wave supercontinuum generation. Opt. Express **17**, 21497 (2009)

33. Baronio, F., Conforti, M., Degasperis, A., Lombardo, S., Onorato, M., Wabnitz, S.: Vector rogue waves and baseband modulation instability in the defocusing regime. Phys. Rev. Lett. **113**, 034101 (2014)

34. Baronio, F., Chen, S.H., Grelu, P., Wabnitz, S., Conforti, M.: Baseband modulation instability as the origin of rogue waves. Phys. Rev. A **91**, 033804 (2015)

35. Wang, X., Wei, J., Wang, L., Zhang, J.L.: Baseband modulation instability, rogue waves and state transitions in a deformed Fokas–Lenells equation. Nonlinear Dyn. **97**, 343–353 (2019)